The Journal of Chemical Physics

Sampling initial positions and momenta for nuclear trajectories from quantum mechanical distributions

Cite as: J. Chem. Phys. **154**, 074115 (2021); https://doi.org/10.1063/5.0039592
Submitted: 04 December 2020 . Accepted: 27 January 2021 . Published Online: 19 February 2021

Yuxuan Yao, William L. Hase, Giovanni Granucci, and Maurizio Persico

The Journal of Chemical Physics ARTICLE scitation.org/journal/jcp

Sampling initial positions and momenta for nuclear trajectories from quantum mechanical distributions

Cite as: J. Chem. Phys. 154, 074115 (2021); doi: 10.1063/5.0039592
Submitted: 4 December 2020 • Accepted: 27 January 2021 •
Published Online: 19 February 2021

Yuxuan Yao,[1] William L. Hase,[1,a)] Giovanni Granucci,[2] and Maurizio Persico[b)]

AFFILIATIONS

[1] Department of Chemistry and Biochemistry, Texas Tech University, Lubbock, Texas 79409, USA
[2] Department of Chemistry and Industrial Chemistry, University of Pisa, v. G. Moruzzi 13, Pisa, Italy

[a)] Deceased.
[b)] **Author to whom correspondence should be addressed:** maurizio.persico@unipi.it

ABSTRACT

We compare algorithms to sample initial positions and momenta of a molecular system for classical trajectory simulations. We aim at reproducing the phase space quantum distribution for a vibrational eigenstate, as in Wigner theory. Moreover, we address the issue of controlling the total energy and the energy partition among the vibrational modes. In fact, Wigner's energy distributions are very broad, quite at variance with quantum eigenenergies. Many molecular processes depend sharply on the available energy, so a better energy definition is important. Two approaches are introduced and tested: the first consists in constraining the total energy of each trajectory to equal the quantum eigenenergy. The second approach modifies the phase space distribution so as to reduce the deviation of the single mode energies from the correct quantum values. A combination of the two approaches is also presented.

I. INTRODUCTION

Classical trajectory simulations are widely employed in studying atomic-level dynamics of thermal reactions and post-reaction properties, such as possible product channels and product energy partitioning, when truly quantum effects can be neglected.[1–8] Nonadiabatic trajectory simulations, for instance within the surface hopping approach or the recently introduced exact factorization of electronic and nuclear motions, are also very useful to describe excited state dynamics and photochemical reactions.[9–11]

Both in thermal and in excited state studies, a frequently applied strategy is to run a swarm of many energy conserving trajectories, starting with initial conditions (positions **q** and momenta **p**) sampled according to a quantum mechanical (QM) probability distribution. To simulate the excited state nonadiabatic dynamics, after sampling the coordinates **q** and **p** for a vibrational state in the ground electronic potential energy surface (PES), a vertical excitation is performed to another PES.[9,10] We also showed how to produce a microcanonical ensemble of quantum vibrational states of given energy around a potential minimum or a conical intersection point.[12] The proper choice of initial conditions can be crucial to obtain accurate results.[1–3,7,8] In fact, reproducing the QM **q** and **p** distributions guarantees the correct dynamical behavior of the classical swarm of trajectories, at least to first order in time, according to the Ehrenfest theorem. Moreover, full agreement with quantum dynamics is ensured with quadratic potentials.[13,14] For instance, López and McCoy[2] found a better agreement between classical trajectories and quantum dynamics simulations of Ne + Ar_2 collisions by using the quantum distributions of **q** and **p** instead of the classical ones. Also, in photodynamics simulations, the excitation probability dependence on the molecular geometry should be taken into account, to correctly reproduce the experimental conditions (namely, monochromatic

light vs ultrashort pulses).[9,14] Then, the **q** distribution can deeply affect the dynamics, for instance, in the case of symmetry forbidden transitions[8,15] or when the exciting wavelength falls in a band tail.[8]

Sampling the Wigner function $W(\mathbf{p}, \mathbf{q})$[16,17] relative to the initial quantum state yields the correct distributions for both **q** and **p** separately. Moreover, Wigner sampling has the advantage that the classical energy $E_i^{(cl)}(q_i, p_i)$ for each vibrational mode i, averaged over many phase space points, equals the quantum expectation value. The same is true, of course, for the total energy $E_{tot}^{(cl)} = \sum_i E_i^{(cl)}$. However, even in the case of QM eigenstates, the distribution of the $E_i^{(cl)}$ and $E_{tot}^{(cl)}$ values can be quite broad. In the common case of energy conserving dynamics, the energy of any single trajectory may be much lower or higher than the QM one. This is a severe drawback when the total available energy determines the accessibility of crucial portions of the PESs, such as transition states or conical intersections. Moreover, the correct distribution of energy in the vibrational modes can also be important, for instance, when vibrational or vibronic excitation results in vibrational predissociation. The concentration of vibrational energy (or the lack thereof) in particular bonds or functional groups involved in the reaction is obviously crucial. In reactive scattering studies, a common procedure is to set the energy of the reactants to a selected vibrational level. However, Cotton and Miller[18] showed that the assignment of both reactants and products to quantum vibrational levels by Gaussian windowing in the energy scale improves the agreement with quantum results. Using Wigner's energy distribution [Eq. (12)] for windowing instead of a narrower Gaussian yielded much worse results.[18] In general, we expect ultrafast processes to be most sensitive to the **q** and **p** initial distributions, while long times result in statistical conditions where energy considerations prevail.

In this paper, we propose different ways to modify the **q** and **p** quantum distributions in order to obtain a better energy resolution in sampling the initial conditions for trajectory simulations. One of these approaches has been already applied in the previous work,[4,19] and the others are new. We shall examine two ways to modify Wigner sampling by imposing a fixed total classical energy $E_{tot}^{(cl)}$, i.e., to achieve strictly microcanonical conditions. Moreover, we shall see how to get $E_{tot}^{(cl)}$ and $E_i^{(cl)}$ distributions that average to the correct QM value and peak around it, with a moderate change of the q_i and p_i marginal distributions corresponding to the Wigner function. These two approaches will be indicated as the "microcanonical"one and the "mode specific" one, respectively. A combination of both approaches will be also presented. Very often, it is assumed that the initial vibrational state is the lowest one, corresponding to the zero point energy (ZPE) level: this is correct for the excited state dynamics of fairly rigid molecules and for simulations of thermal chemistry starting at a transition state (TS). The vibrational wavefunctions and energies are usually obtained by a normal mode treatment, within the harmonic approximation. For instance, in previous work on the $C_2H_5F \rightarrow HF + C_2H_4$ reaction, the ZPE Wigner function was used to sample initial coordinates and momenta for the TS and worked well.[19] For the sake of simplicity, in this work, we shall limit ourselves to the ZPE level in the harmonic approximation.

II. THEORY AND ALGORITHMS

The Wigner correlated pseudo-distribution of a coordinate q and its conjugate momentum p is[16,17]

$$W(q,p) = \frac{1}{\pi\hbar}\int_{-\infty}^{+\infty} \psi^*(q+x)\psi(q-x)\, e^{2ipx/\hbar}\, dx, \tag{1}$$

where $\psi(q)$ is the wavefunction in position space. The function $W(q, p)$ is the appropriate weight to compute the average of any observable that depends on q and p. So, for instance, if ψ is an eigenstate with eigenvalue $E^{(qm)}$, the classical energy

$$E^{(cl)}(q,p) = V(q) + \frac{p^2}{2m} \tag{2}$$

averages to $E^{(qm)}$:

$$\left\langle E^{(cl)} \right\rangle = \int_{-\infty}^{+\infty} W(q,p)\, E^{(cl)}(q,p)\, dq\, dp = E^{(qm)}. \tag{3}$$

These relationships can be generalized straighforwardly to the multi-dimensional case. In particular, if ψ is a product of single coordinate factors ψ_i, all the variables we have introduced acquire a subscript i: the abovementioned equations hold for q_i, p_i, $E_i^{(cl)}$, and $E_i^{(qm)}$, while the total energy is

$$E_{tot}^{(qm)} = \sum_{i=1}^{N_C} E_i^{(qm)}. \tag{4}$$

The multi-dimensional Wigner function is also factorized:

$$W(\mathbf{q},\mathbf{p}) = \prod_{i=1}^{N_C} W^{(i)}(q_i, p_i), \tag{5}$$

where N_C is the number of coordinates. This is the case for molecular vibrations in the harmonic approximation, where the q_i's are the normal coordinates, expressed as linear combinations of mass-weighted Cartesian displacements. The energy expression for the i-th mode is $E_i^{(cl)} = (\omega_i^2 q_i^2 + p_i^2)/2$, where ω_i is the (angular) frequency. It is convenient to convert to dimensionless coordinates:

$$Q_i = \sqrt{\frac{\omega_i}{\hbar}}\, q_i \quad \text{and} \quad P_i = \frac{1}{\sqrt{\hbar\omega_i}}\, p_i. \tag{6}$$

The energy expression is then

$$E_i^{(cl)} = \frac{\hbar\omega_i}{2}\left(Q_i^2 + P_i^2\right), \tag{7}$$

which means Q and P also have the same role in the QM hamiltonian and, therefore, the same probability distributions. Moreover, the eigenfunctions (Hermite functions) are formally the same for all modes:

$$\psi_n(Q_i) = \pi^{-1/4}(2^n n!)^{-1/2} e^{-Q_i^2/2}\, H_n(Q_i), \tag{8}$$

where n is the quantum number. The same holds for the Wigner functions:[17]

$$W_n(Q_i,P_i) = \pi^{-1}\, e^{-(Q_i^2+P_i^2)}\, (-1)^n\, L_n(2Q_i^2+2P_i^2), \tag{9}$$

where L_n is the n-th Laguerre polynomial. The Wigner function is now the same for all modes and only depends on $Q_i^2 + P_i^2 = 2E_i^{(cl)}/(\hbar\omega_i)$. As a general property, the marginal distributions one obtains by integrating the Wigner function over P_i or Q_i are just the QM $\rho_n(Q_i)$ and $\rho_n(P_i)$ probability densities, respectively:

$$\int_{-\infty}^{+\infty} W_n(Q_i,P_i)\, dP_i = \rho_n(Q_i) = |\psi_n(Q_i)|^2, \tag{10}$$

$$\int_{-\infty}^{+\infty} W_n(Q_i,P_i)\, dQ_i = \rho_n(P_i) = |\tilde{\psi}_n(P_i)|^2. \tag{11}$$

We note that while ρ_n is nowhere negative, there are regions where $W_n(Q_i, P_i) < 0$, except when $n = 0$. This problem can be dealt with in different ways, but none of them is quite satisfactory. For instance, the Wigner function can be modified to eliminate the negative values as proposed by Husimi,[20] but then, it does not yield the correct marginal distributions for Q_i and P_i and the agreement with quantum dynamics was found to downgrade in tests on a conical intersection model.[3] For finite temperature simulations, one could sample the Wigner function W_T corresponding to the Boltzmann distribution for a harmonic oscillator, which is nowhere negative.[17] However, except with very low mode frequencies ($\hbar\omega_i \ll K_BT$), the energy distribution associated with W_T has the same drawbacks already highlighted in the introduction for the state specific one, W_n: it is a broad distribution not peaked at the quantum eigenvalues (just consider that, in the limiting case of high frequency, $W_T \simeq W_n$ with $n = 0$). The method presented in Sec. II B can be easily applied to vibrationally excited states because it is based on the marginal distributions instead of the Wigner function. It can also treat the finite temperature case, by sampling the appropriate distributions for the relevant vibrational states and then weighting them with the Boltzmann factors. However, low frequencies often belong to very anharmonic vibrations. In small systems, the Wigner sampling of anharmonic modes was performed,[2,3] but large and floppy molecular systems are better dealt with by sampling thermostated trajectories. In the latter case, quantum corrections for the high frequency modes can improve the accuracy[8,21,22] because the classical thermal motion underestimates the average displacement from equilibrium when $\hbar\omega/2 > K_BT$.

By specializing to the $n = 0$ state, we get

$$W_0(Q_i,P_i) = \pi^{-1}\, e^{-(Q_i^2+P_i^2)} = \rho(Q_i)\,\rho(P_i) = \pi^{-1}\, e^{-2E_i^{(cl)}/(\hbar\omega_i)}. \tag{12}$$

The Wigner function in this case is simply the product of the Q and P densities, which are, in turn, the same Gaussian function $\rho(X) = \pi^{-1/2}\, e^{-X^2}, X = Q, P$. The classical energy distribution $\rho_{E,i}(E_i^{(cl)})$ is exponential, averaging to the ZPE $E_{i,0} = \hbar\omega_i/2$ but with the mode at $E_i^{(cl)} = 0$ and a substantial tail at higher energies.

A. Microcanonical approach

We present two methods that will be labeled microcanonical one-vector (MOV) and microcanonical two-vector (MTV), respectively.

1. One-vector sampling

The most direct way to perform a microcanonical sampling is to partition the desired total energy randomly, i.e., in our case, $E_{tot}^{(qm)}$, into the N_C modes. This can be achieved by generating random unit vectors $\mathbf{X}$ of dimension N_C and setting

$$E_i^{(cl)} = E_{tot}^{(qm)}\, X_i^2. \tag{13}$$

We have tested two algorithms that generate random unit vectors, the orthant method of Bunker and Hase[23] and the one proposed by Muller.[24] We used the latter throughout this work because we found it slightly faster in our implementation, based on the Box–Muller transform.[25]

Once a set of $E_i^{(cl)}$ energies $\mathbf{E}^{(cl)} = (E_1^{(cl)}, E_2^{(cl)}, \ldots, E_{N_C}^{(cl)})$ has been generated by the unbiased microcanonical sampling, we submit it to screening through von Neumann's rejection method, according to the N_C-dimensional Wigner distribution:

$$W(\mathbf{E}^{(cl)}) = \pi^{-N_C} \prod_{i=1}^{N_C} e^{-2E_i^{(cl)}/(\hbar\omega_i)}. \tag{14}$$

The maximum value of $W(\mathbf{E}^{(cl)})$ is obtained when the whole $E_{tot}^{(qm)}$ energy is attributed to the highest frequency mode, so $max(W) = \pi^{-N_C}\, e^{-2E_{tot}^{(qm)}/[\hbar\, max(\omega_i)]}$. The rejection method is then applied by comparing a random number $R \in [0, 1]$ with the function $W(\mathbf{E}^{(cl)})/max(W)$.

The $\mathbf{Q}$ and $\mathbf{P}$ values are then determined by Eq. (7), which is the constraint to which undergoes the random choice of each Q_i, P_i pair. In practice, we randomly choose $\theta \in [0, 2\pi]$, and we set

$$Q_i = \sqrt{\frac{2E_i^{(cl)}}{\hbar\omega_i}}\, \sin\theta \quad \text{and} \quad P_i = \sqrt{\frac{2E_i^{(cl)}}{\hbar\omega_i}}\, \cos\theta, \tag{15}$$

2. Two-vector sampling

Another way to perform microcanonical sampling is to determine the Q_is and P_is directly, by relating them to the components of a unit vector $\mathbf{X}$ of dimension $2N_C$:

$$Q_i = \sqrt{\frac{2E_{tot}^{(qm)}}{\hbar\omega_i}}\, X_{2i-1} \quad \text{and} \quad P_i = \sqrt{\frac{2E_{tot}^{(qm)}}{\hbar\omega_i}}\, X_{2i}. \tag{16}$$

We see, through Eq. (7), that $E_i^{(cl)} = E_{tot}^{(qm)}(X_{2i-1}^2 + X_{2i}^2)$ and the total energy is again $E_{tot}^{(qm)}$. The sampled unit vectors are submitted to von Neumann's rejection as in the one-vector case, to approximate the Wigner distribution. This method was discussed in detail by Sun and Hase.[19] A procedure to allow for moderate anharmonicities still keeping the total energy constraint is described by Peslherbe

et al.,[26] Sec. II.A.3.a. The same recipe can be applied to the MMS approach (see Sec. II C).

B. Mode specific approach

The gist of the mode specific approach (MS) is to reduce the variance of the single mode $E_i^{(cl)}$ energies around their QM targets $E_i^{(qm)}$, while ensuring that $\langle E_i^{(cl)} \rangle = E_i^{(qm)}$. Of course, these two conditions also affect the total energy $E_{tot}^{(cl)}$ in a similar way. To this aim, we modify the QM distribution by introducing the bias factor

$$b_i(E_i^{(cl)}) = e^{-(E_i^{(cl)} - E_i^{(b)})^2/(2\sigma^2 E_i^{(qm)\,2})}. \tag{17}$$

This function is a Gaussian with standard deviation $\sigma E_i^{(qm)}$, where σ is a user-defined parameter: a smaller value of σ not only reduces the spread of $E_i^{(cl)}$ values around the correct $E_i^{(qm)}$ energy but also entails a more marked departure from the QM distribution of Q_i and P_i. The $E_i^{(b)}$ energy around which the Gaussian is centered is automatically adjusted to satisfy the equality $\langle E_i^{(cl)} \rangle = E_i^{(qm)}$.

The distribution of Q_i and P_i to which we apply the bias could be the Wigner function as in the MOV and MTV cases or just the product of the two marginal distributions, $\rho(Q_i)\rho(P_i)$. In fact, since in both cases, we shall obtain $\langle E_i^{(cl)} \rangle = E_i^{(qm)}$, we are not compelled to use the Wigner function. We then prefer the marginal distributions in view of applications to excited vibrational states, to avoid the problem of negative values in the Wigner functions. With $n = 0$, of course, the two alternatives just coincide. The function from which we sample Q_i and P_i is then

$$\rho_i^{(MS)}(Q_i, P_i) = \rho(Q_i)\,\rho(P_i)\,b_i(Q_i, P_i), \tag{18}$$

where the bias factor b_i can be considered a function of Q_i and P_i through relationship (7). On the other hand, with $n = 0$, the product $\rho(Q_i)\rho(P_i)$ is an exponential function of $E_i^{(cl)}$, as shown by Eq. (12). Then, $\rho_i^{(MS)}$ as a function of $E_i^{(cl)}$ is also a Gaussian with the maximum at $E_i^{(cl)} = E_i^{(b)} - \sigma^2 E_i^{(qm)}$, which yields a first guess for the $E_i^{(b)}$ parameter, $E_i^{(b)} = (1 + \sigma^2)E_i^{(qm)}$. In practice, Q_i and P_i are first chosen by Box–Muller sampling[25] and then von Neumann's rejection is applied to the $b_i(E_i^{(cl)})$ function. Once the averages $\langle E_i^{(cl)} \rangle$ have been determined for all modes, the $E_i^{(b)}$ parameters are changed to $E_i^{(b)\prime} = E_i^{(b)} + E_i^{(qm)} - \langle E_i^{(cl)} \rangle$ and the sampling is repeated. The procedure is iterated until convergence of all the $\langle E_i^{(cl)} \rangle$ to the respective $E_i^{(qm)}$.

With the mode specific sampling, one gets $\langle E_{tot}^{(cl)} \rangle = E_{tot}^{(qm)}$, and the $E_{tot}^{(cl)}$ values can be pushed to gather around the quantum eigenvalue as closely as desired by choosing σ small enough, at the price of an increasing distortion of the quantum $\rho(Q)$ and $\rho(P)$ distributions. However, the sampling is not strictly microcanonical.

C. Combined microcanonical and mode specific approach

In principle, it is very simple to combine the microcanonical approach (MOV or MTV) with the mode specific one (MS) to benefit of the advantages of both. In fact, the distribution generated microcanonically can be altered by applying a bias as seen in Sec. II B: this approach will be called "microcanonical mode specific" (MMS). However, a generated unit vector must be accepted or rejected as a whole; therefore, the algorithm is a bit more complicated. We generate the **Q** and **P** vectors as in the MTV method. Then, we evaluate the associated probability density as

$$\rho^{(MMS)}(\mathbf{Q}, \mathbf{P}) = \prod_{i=1}^{N_C} \rho_i^{(MS)}(Q_i, P_i) \tag{19}$$

and we use von Neumann's rejection to keep or discard the **Q**, **P** vectors. The problem is we did not find a closed formula for the maximum value of $\rho^{(MMS)}(\mathbf{Q}, \mathbf{P})$ with the microcanonical constraint. However, given a provisional maximum value M, the rejection algorithm works correctly if $\rho^{(MMS)}(\mathbf{Q}, \mathbf{P})/M \le 1$ for all the sampled **Q**, **P** vectors. Since M is not the global maximum of the function, during the sampling, we may encounter a $\rho^{(MMS)}$ value M' exceeding M, in which case M is reset to $1.05 \cdot M'$ and the sampling is restarted afresh.

III. TESTING AND COMPARING THE SAMPLING APPROACHES

We tested the methods described in Sec. II on four molecules: water, methane, the transition state of the $C_2H_5F \rightarrow HF + C_2H_4$ reaction ($C_2H_5F^{\ddagger}$), and *trans*-azomethane. We always considered the ground vibrational state, with $n = 0$ for all modes. All calculations sampled $N_S = 10^5$ phase space points, with one exception (the MMS sampling of $C_2H_5F^{\ddagger}$, for which $N_S = 10^4$). We shall first analyze the $C_2H_5F^{\ddagger}$ results in detail, and next, we shall extend the discussion to the other molecules, focusing on the influence of the number of vibrational modes, N_C.

In Tables II–V, we report five statistical parameters that characterize the $E_{tot}^{(cl)}$, $E_i^{(cl)}$, Q_i, and P_i distributions. The total energy $E_{tot}^{(cl)}$ obtained by microcanonical sampling (MOV, MTV, or MMS) is simply equal to $E_{tot}^{(qm)}$, while by the Wigner or mode specific samplings, it averages (approximately, with finite N_S) to the same value. Therefore, we only report its relative standard deviation, defined as

$$\mathrm{RSTD}(E_{tot}^{(cl)}) \equiv \frac{\sqrt{\langle E_{tot}^{(cl)\,2} \rangle - \langle E_{tot}^{(cl)} \rangle^2}}{E_{tot}^{(qm)}}. \tag{20}$$

The $E_i^{(cl)}$ energies are not guaranteed to average to their quantum counterparts $E_i^{(qm)}$ by the MOV and MTV approaches, so we list two parameters. One is the unsigned relative error with respect to the $E_i^{(qm)}$ target, averaged over all modes:

$$\mathrm{AURE}(E_i^{(cl)}) \equiv \frac{1}{N_C}\sum_i \frac{\left|\left\langle E_i^{(cl)}\right\rangle - E_i^{(qm)}\right|}{E_i^{(qm)}}. \tag{21}$$

The other parameter concerning the $E_i^{(cl)}$ energies is their relative standard deviation, also averaged over all modes:

$$\mathrm{ARSTD}(E_i^{(cl)}) \equiv \frac{1}{N_C}\sum_i \frac{\left\langle E_i^{(cl)2}\right\rangle - \left\langle E_i^{(cl)}\right\rangle^2}{E_i^{(qm)}}. \tag{22}$$

The Q_i and P_i values and their odd powers always average to zero, within the accuracy allowed by the finite N_S. For the same reason, $\langle Q_i^m\rangle \simeq \langle P_i^m\rangle$ with even m. We, therefore, report the second and fourth moments for Q_i and P_i together, again averaged over all modes:

$$\left\langle Q^m\right\rangle \equiv \left\langle P^m\right\rangle \equiv \frac{1}{N_C}\sum_i \frac{\langle Q_i^m\rangle + \langle P_i^m\rangle}{2} \tag{23}$$

with $m = 2, 4$.

In each table, the first line reports the values obtained by pure Wigner sampling, without constraints or biases. Some of them are independent on the mode frequencies and theoretically (i.e., barring the uncertainty due to finite N_S) should be $\mathrm{AURE}(E_i^{(cl)}) = 0$, $\mathrm{ARSTD}(E_i^{(cl)}) = 1$, $\left\langle Q^2\right\rangle = 1/2$, and $\left\langle Q^4\right\rangle = 3/4$. The relative standard deviation of $E_{tot}^{(cl)}$ depends on the frequencies as

$$\mathrm{RSTD}(E_{tot}^{(cl)}) = \mathrm{ARSTD}(E_i^{(cl)})\sqrt{\sum_i \omega_i^2}\Big/\left(\sum_i \omega_i\right). \tag{24}$$

The statistical values reported in the tables closely agree with this formula.

In Table S1 and in Fig. S2, we show, for reference, the results obtained by the different methods for a single harmonic oscillator. Of course, here, the $E_{tot}^{(cl)}$ and $E_i^{(cl)}$ values are just the same. The microcanonical methods (MOV, MTV, and MMV) all yield, by construction, the right energy and the distribution of Q_i and P_i pertaining to the classical harmonic oscillator; hence, $\left\langle Q^2\right\rangle = 1/2$ and $\left\langle Q^4\right\rangle = 3/8$. In this limiting case, the microcanonical sampling completely overrides the Wigner distribution. With several modes, as we shall see, the effect of the $E_{tot}^{(cl)} = E_{tot}^{(qm)}$ constraint is much milder. The MS method yields a distribution of energies with the $\left\langle E_{tot}^{(cl)}\right\rangle = E_{tot}^{(qm)}$ and a standard deviation that increases with the σ parameters (for σ small enough, $\mathrm{ARSTD}(E_i^{(cl)}) \simeq \sigma$). The Q_i and P_i distributions tend to the classical ones for small σ and to the QM ones for large σ.

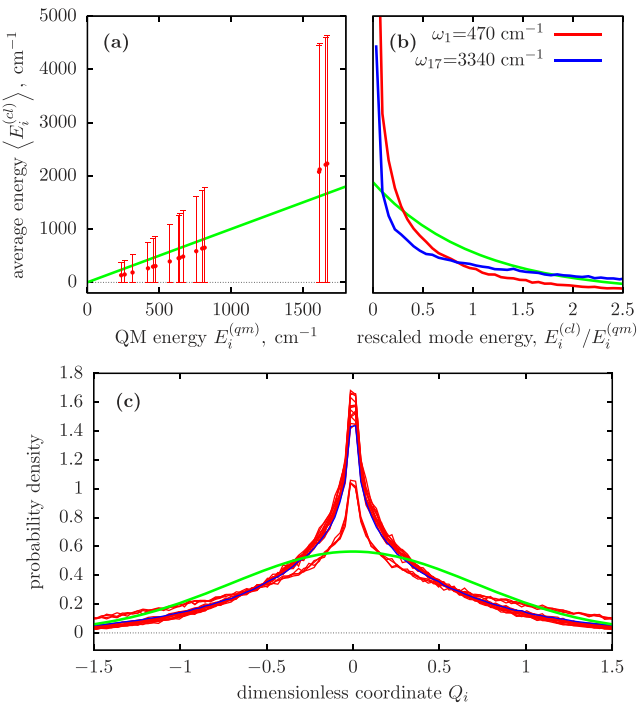

FIG. 1. Sampling algorithm MOV for $C_2H_5F^{\ddagger}$. 10^5 samples. (a) Average mode energies and standard deviations. Most standard deviations were larger than the average energies, so the corresponding error bars were displaced so as to start at zero energy. (b) Rescaled energy distributions for the lowest and highest frequency modes. (c) Q_i distributions for all modes. The green lines mark the exact QM energies and distributions, respectively.

A. $C_2H_5F^{\ddagger}$ results

The fluoroethane transition state, $C_2H_5F^{\ddagger}$, has 17 non imaginary frequencies, reported in Table I, as computed at the

TABLE I. Vibrational frequencies of water,[28] methane,[28] $C_2H_5F^{\ddagger}$,[27] and *trans*-azomethane.[29]

Molecule	N_C	Frequencies, cm^{-1} (degeneracy)
Water	3	1595, 3657, 3756
Methane	9	1306 (3), 1534 (2), 2917, 3019 (3)
$C_2H_5F^{\ddagger}$	17	470, 519, 629, 843, 914, 947, 1147, 1270, 1286, 1333, 1516, 1599, 1633, 3226, 3235, 3319, 3340
Azomethane	24	214, 222, 312, 353, 591, 919, 1008, 1027, 1111, 1112, 1179, 1381, 1384, 1416, 1437, 1440, 1447, 1583, 2925, 2926, 2977, 2981, 2988, 2989

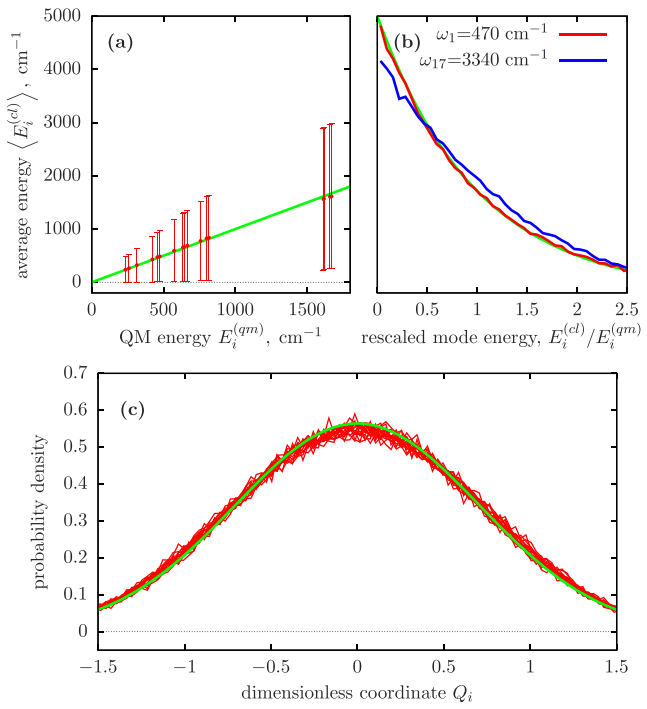

FIG. 2. Sampling algorithm MTV for $C_2H_5F^{\ddagger}$. 10^5 samples. (a)–(c) Same as in Fig. 1.

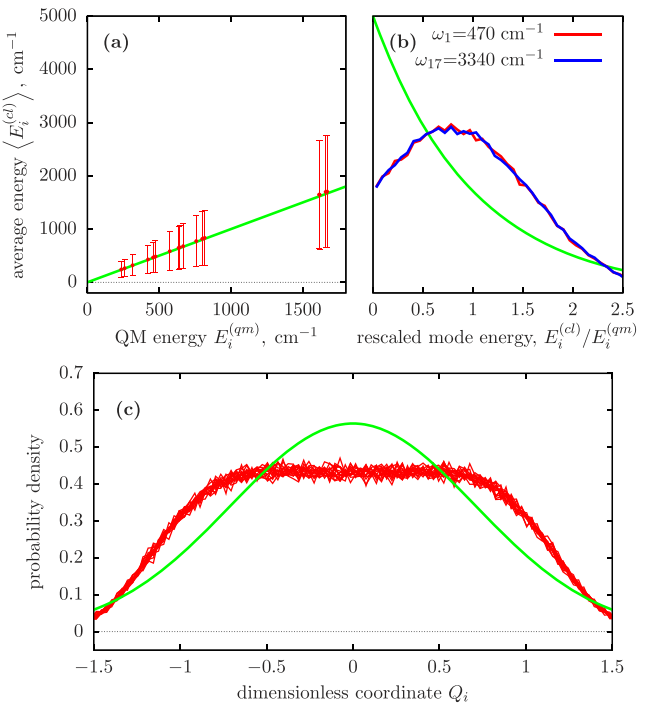

FIG. 4. Sampling algorithm MS for $C_2H_5F^{\ddagger}$. Bias parameter σ = 0.8, 10^5 samples. (a)–(c) Same as in Fig. 1.

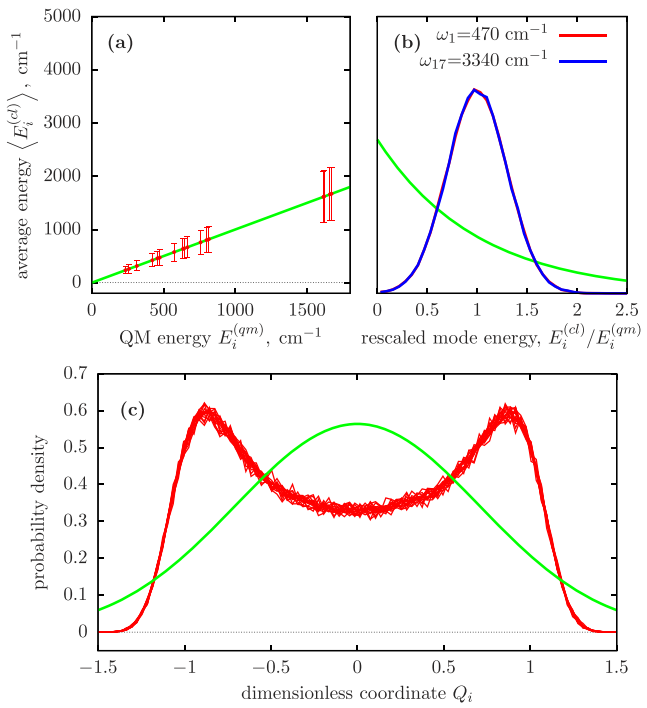

FIG. 3. Sampling algorithm MS for $C_2H_5F^{\ddagger}$. Bias parameter σ = 0.3, 10^5 samples. (a)–(c) Same as in Fig. 1.

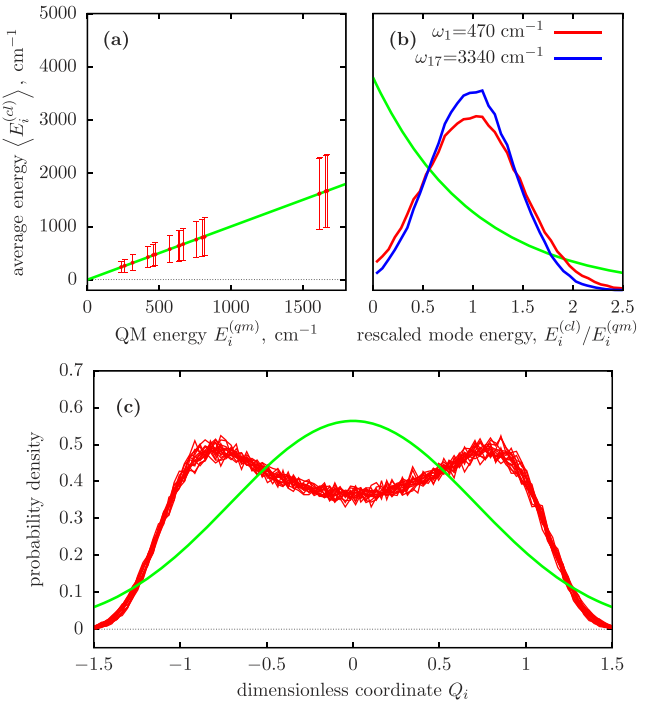

FIG. 5. Sampling algorithm MMS for $C_2H_5F^{\ddagger}$. Bias parameter σ = 0.5. 13 low frequency modes and 4 high frequency ones are treated separately. (a)–(c) Same as in Fig. 1.

MP2/6-31G* level of theory.[27] Figure S1 shows the results of Wigner sampling, for comparison with Figs. 1–5 that share the same scheme. In panel (a), we plot the $\langle E_i^{(cl)} \rangle$ averages with the relative standard deviations (STD) as error bars. In panel (b), we show the $E_i^{(cl)}$ distribution for the lowest and the highest frequency modes, as obtained by hystograms of the sampled points, compared with the theoretical Wigner distribution, Eq. (12). Finally, in panel (c), we have the Q_i distributions, again compared with the theoretical one.

The MOV results (see Fig. 1 and Table II) show a noticeable departure from the Wigner ones. The $\langle E_i^{(cl)} \rangle$ energies (a) lie below the corresponding eigenvalues $E_i^{(qm)}$ for low frequencies and above for high frequencies, with a large AURE. The Q_i distributions deviate considerably from the ideal Gaussian shape. In comparison, the other microcanonical sampling, MTV, behaves much better (see Fig. 2). The $\langle E_i^{(cl)} \rangle$ energies are acceptably close to the $E_i^{(qm)}$ eigenvalues, and the distorsion of the $E_i^{(cl)}$ and Q_i distributions is quite modest. The difference between the MOV and MTV Q_i distributions is also reflected in the values of $\langle Q^2 \rangle$ and $\langle Q^4 \rangle$. Of course, both algorithms alter the Q_i, P_i and $E_i^{(cl)}$ distributions because of the microcanonical constraint, but in a different way. In fact, when using the MTV algorithm, once the constraint is taken into account, there are still $2N_C - 1$ degrees of freedom to be chosen according to the Wigner distribution, while in the MOV algorithm, the degrees of freedom reduce to $N_C - 1$. Therefore, in MTV, the microcanonical constraint affects the Q_i and P_i distributions less severely than in MOV. Overall, the MTV algorithm is preferable, despite being more time-consuming because it generates unit vectors of dimension $2N_C$ instead of N_C.

The application of the mode specific (MS) approach depends on the choice of the σ parameter. In Table II, we list results for $\sigma \in [0.2, 0.8]$, and in Figs. 3 and 4, we show the distributions obtained with $\sigma = 0.3$ and 0.8. As anticipated in Sec. II B, the bias affects the distributions more noticeably for small values of σ. This means, the smaller the σ, the narrower the $E_i^{(cl)}$ distributions, with the relative standard deviation ARSTD not far from σ. By construction, the error on the $\langle E_i^{(cl)} \rangle$ energies, AURE, is approximately zero, with statistical deviations increasing with σ. The total energy dispersion $\mathrm{RSTD}(E_{tot}^{(cl)})$ depends on the mode frequencies as in the case of Wigner distribution, Eq. (24), so it is approximately proportional to σ. The Q_i distributions deviate from the QM Gaussian, and with small σ, they become bimodal as in the classical harmonic oscillator. However, with larger σ, they are not too far from the QM shape. This behavior affects the fourth moment $\langle Q^4 \rangle$ much more than the second moment $\langle Q^2 \rangle$. Since σ rules the trade-off between matching the QM Q_i and P_i distributions or the $E_i^{(qm)}$ mode energies more closely, its choice depends on how important it is to satisfy either of the two requirements to simulate the process under study, as already discussed in the introduction.

Finally, Figs. 5 and 6 and Fig. S3 illustrate the application of the combined approach MMS. While the simple MS algorithm is very fast (see the last column of Table II), the MMS algorithm suffers of the need to generate many unit vectors as the MTV one, plus a high rejection rate that increases with smaller σ values: the sampling with $\sigma = 0.5$ is about 10^6 times slower than with $\sigma = 0.8$. To circumvent this difficulty, we partitioned the $C_2H_5F^{\ddagger}$ vibrational modes in two sets, 13 with low frequency and 4 with high frequency, and we applied the MMS sampling to each set separately. Figure 5 shows the results obtained with this "split" option and $\sigma = 0.5$, and

TABLE II. Results obtained with different methods and parameters for $C_2H_5F^{\ddagger}$.

		$E_{tot}^{(cl)}$	$E_i^{(cl)}$	$E_i^{(cl)}$			CPU time
Method	N_C[a]	RSTD	AURE	ARSTD	$\langle Q^2 \rangle = \langle P^2 \rangle$	$\langle Q^4 \rangle = \langle P^4 \rangle$	(s)
Wigner	17	0.283	0.002	1.00	0.499	0.747	<1
MOV	17	0.000	0.320	1.05	0.414	0.716	1210
MTV	17	0.000	0.028	0.96	0.507	0.733	$2.18 \cdot 10^4$
MS, $\sigma = 0.2$	17	0.057	0.001	0.20	0.500	0.390	~1
MS, $\sigma = 0.3$	17	0.085	0.001	0.30	0.500	0.409	~1
MS, $\sigma = 0.4$	17	0.111	0.007	0.39	0.503	0.437	~1
MS, $\sigma = 0.5$	17	0.133	0.004	0.47	0.501	0.459	~1
MS, $\sigma = 0.6$	17	0.152	0.013	0.53	0.506	0.491	~1
MS, $\sigma = 0.8$	17	0.180	0.020	0.63	0.510	0.540	~1
MMS, $\sigma = 0.5$	17	0.000	0.004	0.46	0.500	0.454	$1.30 \cdot 10^5$[b]
MMS, $\sigma = 0.5$	13 l	0.000	0.009	0.45	0.502	0.454	3204
MMS, $\sigma = 0.5$	4 h	0.000	0.001	0.41	0.500	0.439	~1
MMS, $\sigma = 0.8$	17	0.000	0.011	0.61	0.503	0.519	$1.06 \cdot 10^4$

[a] $N_C \equiv$ number of modes. The specification "l" (or "m" or "h") means that the subset of the N_C lowest (or intermediate or highest) frequency coordinates is treated separately.
[b] This calculation was run with $N_S = 10^4$ instead of the standard $N_S = 10^5$.

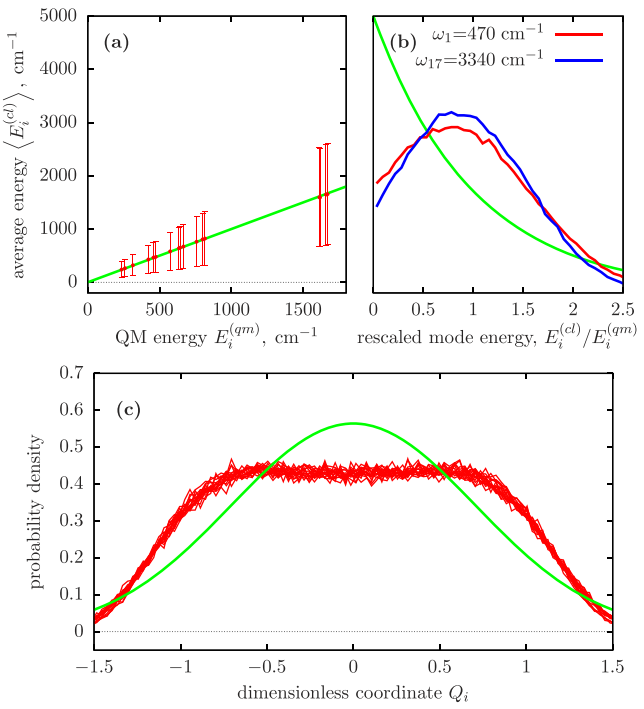

FIG. 6. Sampling algorithm MMS for $C_2H_5F^{\ddagger}$. Bias parameter σ = 0.8. (a)–(c) Same as in Fig. 1.

Fig. S3 shows those obtained for all 17 modes together (but with only 10^4 sampled points). The difference between the two treatments is minor, but, of course, the split option forces the modes of each set to obey the microcanonical constraint separately. The reduction in computing time is dramatic, and the split option can be easily applied to the MOV and MTV methods as well. The distributions of $E_i^{(cl)}$, Q_i, and P_i obtained with the MMS sampling turn out to be similar to those of MS, for the same value of σ: in other words, the microcanonical constraint has a minor effect on such distributions, just as in the MTV approach.

IV. WATER, METHANE, AND AZOMETHANE RESULTS

Water, methane, and azomethane count 3, 9, and 24 vibrational modes, respectively, so we can examine how the different algorithms behave at both lower and higher dimensions with respect to $C_2H_5F^{\ddagger}$. The vibrational frequencies of the three compounds are listed in Table I. For azomethane, to apply the MTV and MMS algorithms, we partitioned the 24 modes in three subsets of 5, 13, and 6 modes: low frequencies, up to 591 cm^{-1}; intermediate, from 919 cm^{-1} to 1583 cm^{-1}; and high, from 2925 cm^{-1} to 2989 cm^{-1}. The general features already discussed in Sec. III A are confirmed by the results shown in Tables III–V. We shall only discuss some aspects that depend on the dimensionality of the problem.

The dispersion of the total energies in Wigner or MS sampling improves as the number of coordinates increases: for instance, with

TABLE III. Results obtained with different methods and parameters for water.

Method	$E_{tot}^{(cl)}$ RSTD	$E_i^{(cl)}$ AURE	$E_i^{(cl)}$ ARSTD	$\langle Q^2 \rangle = \langle P^2 \rangle$	$\langle Q^4 \rangle = \langle P^4 \rangle$
Wigner	0.608	0.003	1.00	0.500	0.749
MOV	0.000	0.091	0.87	0.482	0.640
MTV	0.000	0.052	0.74	0.510	0.606
MS, σ = 0.2	0.121	0.000	0.20	0.500	0.390
MS, σ = 0.3	0.182	0.001	0.30	0.500	0.409
MS, σ = 0.4	0.238	0.007	0.39	0.504	0.437
MS, σ = 0.5	0.284	0.004	0.47	0.502	0.461
MS, σ = 0.6	0.324	0.012	0.53	0.506	0.491
MS, σ = 0.8	0.383	0.020	0.63	0.510	0.539
MMS, σ = 0.5	0.000	0.009	0.39	0.502	0.435
MMS, σ = 0.8	0.000	0.019	0.52	0.504	0.486

pure Wigner, the parameter RSTD($E_{tot}^{(cl)}$) goes from 0.599 for water to 0.241 for azomethane. In fact, Eq. (24) shows that RSTD($E_{tot}^{(cl)}$) depends not only on the distribution of the ω_i frequencies but also on their number. Assuming all frequencies to be equal, Eq. (24) reduces to RSTD($E_{tot}^{(cl)}$) = ARSTD($E_i^{(cl)}$)/$\sqrt{N_C}$, just an example of the large numbers law. As in MS sampling ARSTD($E_i^{(cl)}$) $\simeq \sigma$, when choosing σ, one can predict that RSTD($E_{tot}^{(cl)}$) $\simeq \sigma/\sqrt{N_C}$.

The quality of the Q_i distributions can be compared by monitoring the $\langle Q^2 \rangle$ and $\langle Q^4 \rangle$ (or $\langle P^2 \rangle$ and $\langle P^4 \rangle$) values. The MOV results, especially $\langle Q^2 \rangle$, deviate considerably from the theoretical values ($\langle Q^2 \rangle$ = 1/2 and $\langle Q^4 \rangle$ = 3/4). The other methods yield $\langle Q^2 \rangle$ sufficiently close to 1/2, so we shall concentrate on $\langle Q^4 \rangle$. The MS results depend on σ and not on the number of coordinates: $\langle Q^4 \rangle$ is too small but increases with σ. The MTV $\langle Q^4 \rangle$ values, on the contrary, steadily improve as the number of coordinates increases (note that, for azomethane, three groups of 5, 13, and 6 coordinates are treated separately). In fact, the large numbers law predicts that the

TABLE IV. Results obtained with different methods and parameters for methane.

Method	$E_{tot}^{(cl)}$ RSTD	$E_i^{(cl)}$ AURE	$E_i^{(cl)}$ ARSTD	$\langle Q^2 \rangle = \langle P^2 \rangle$	$\langle Q^4 \rangle = \langle P^4 \rangle$
Wigner	0.356	0.004	1.00	0.500	0.748
MOV	0.000	0.204	1.10	0.462	0.793
MTV	0.000	0.030	0.91	0.505	0.697
MS, σ = 0.2	0.071	0.000	0.20	0.500	0.390
MS, σ = 0.3	0.107	0.001	0.30	0.500	0.409
MS, σ = 0.4	0.140	0.007	0.39	0.504	0.438
MS, σ = 0.5	0.167	0.003	0.47	0.501	0.459
MS, σ = 0.6	0.189	0.011	0.53	0.506	0.490
MS, σ = 0.8	0.225	0.020	0.63	0.510	0.540
MMS, σ = 0.5	0.000	0.011	0.44	0.502	0.452
MMS, σ = 0.8	0.000	0.022	0.60	0.504	0.516

TABLE V. Results obtained with different methods and parameters for azomethane.

Method	N_C[a]	$E_{tot}^{(cl)}$ RSTD	$E_i^{(cl)}$ AURE	$E_i^{(cl)}$ ARSTD	$\langle Q^2 \rangle = \langle P^2 \rangle$	$\langle Q^4 \rangle = \langle P^4 \rangle$	CPU time (s)
Wigner	24	0.241	0.003	1.00	0.499	0.748	<1
MOV	24	0.000	0.320	1.08	0.414	0.749	$1.14 \cdot 10^5$
MTV	5 l	0.000	0.060	0.85	0.512	0.670	<1
MTV	13 m	0.000	0.011	0.93	0.501	0.700	2
MTV	6 h	0.000	0.004	0.84	0.500	0.642	<1
MS, $\sigma = 0.2$	24	0.048	0.001	0.20	0.500	0.390	~1
MS, $\sigma = 0.3$	24	0.072	0.001	0.30	0.500	0.409	~1
MS, $\sigma = 0.4$	24	0.094	0.007	0.39	0.503	0.438	~1
MS, $\sigma = 0.5$	24	0.113	0.003	0.47	0.501	0.459	~1
MS, $\sigma = 0.6$	24	0.128	0.013	0.53	0.506	0.491	~1
MS, $\sigma = 0.8$	24	0.153	0.020	0.63	0.510	0.540	~1
MMS, $\sigma = 0.5$	5 l	0.000	0.013	0.42	0.503	0.447	2
MMS, $\sigma = 0.5$	13 m	0.000	0.004	0.45	0.500	0.452	1553
MMS, $\sigma = 0.5$	6 h	0.000	0.001	0.43	0.500	0.445	3
MMS, $\sigma = 0.8$	5 l	0.000	0.009	0.57	0.502	0.500	2
MMS, $\sigma = 0.8$	13 m	0.000	0.004	0.61	0.500	0.513	91
MMS, $\sigma = 0.8$	6 h	0.000	0.004	0.58	0.500	0.502	<1

[a] $N_C \equiv$ number of modes. The specification "l" (or "m" or "h") means that the subset of the N_C lowest (or intermediate or highest) frequency coordinates is treated separately.

standard deviation of $E_{tot}^{(cl)}$ would vanish in the limit of $N_C \to \infty$. Hence, the relevance of the constraint $E_{tot}^{(cl)} = \left\langle E_{tot}^{(cl)} \right\rangle = E_{tot}^{(qm)}$ decreases with larger N_C.

The computing times for the methods based on unit vectors (MOV, MTV, and MMS) increase very fast with the number of coordinates. For instance, the MOV calculation for azomethane ($N_C = 24$) is about 100 times longer than that of $C_2H_5F^{\ddagger}$ ($N_C = 17$). Also, by comparing the MMS sampling for $C_2H_5F^{\ddagger}$ (Table II), performed for all modes or two separate subsets, one finds the following approximate time ratios for 4, 13, and 17 modes: $1{:}3 \cdot 10^3{:}10^6$ (we take into account that the 17 modes calculation sampled 10 times less phase space points than the others). Other examples can be extracted from Table V. The pure Wigner sampling and the MS one are much faster and act separately on each mode, so their computational cost is simply proportional to $N_C \cdot N_S$. It is clear that the strictly microcanonical sampling (MOV, MTV, or MMS) cannot be applied to molecules with many more than 10 atoms. In those cases, one must resort to the partition of the modes into subsets, preferably defined on the basis of frequency intervals.

We stress once again that the selection of the best sampling method is a matter of balance between reproducing the QM **q**, **p** distributions or the QM total and single mode energies. For the MS and MMS approaches, the user-defined parameter σ also affects such balance. Such choices depend on the specific process under study. Despite several studies devoted to this problem, we feel that it is not always clear to what extent it is acceptable to deviate from the QM **q**, **p** densities, in particular from the Wigner one. On the other hand, we can suggest a simple way to check whether the uncertainty of $E_{tot}^{(cl)}$ (or any of the $E_i^{(cl)}$s) is too large, when physically they should instead be sharply defined. The basic idea is to monitor the dependence of the computed observables on $E_{tot}^{(cl)}$ (or $E_i^{(cl)}$) across the variability range of the latter. For instance, for the MS method, one can compute the average $\langle O \rangle_+$ of a desired observable over all trajectories with $E_{tot}^{(cl)} > E_{tot}^{(qm)}$ and the average $\langle O \rangle_-$ with $E_{tot}^{(cl)} < E_{tot}^{(qm)}$. If the difference between $\langle O \rangle_+$ and $\langle O \rangle_-$ is unacceptably large, the balance must be shifted toward a better energy definition (smaller σ).

V. CONCLUSIONS

In this work, we introduced new ways to sample the initial conditions, i.e., positions and momenta **q** and **p**, for simulations of molecular dynamics with swarms of nuclear trajectories. We focused on the total classical energy $E_{tot}^{(cl)}$ and on the single vibrational mode energies $E_i^{(cl)}$, which can be crucial to determine the outcome of ground or excited state dynamics.

A full compliance with the quantum mechanical (QM) distributions of **q** and **p**, such as can be obtained by Wigner sampling, yields $E_{tot}^{(cl)}$ and $E_i^{(cl)}$ distributions that spread widely below and above the QM levels. In practice, a compromise must be sought between reproducing the QM distributions for **q** and **p** and getting the right energies. Which trade-off is acceptable depends on the process one wants to simulate. For instance, in the statistical limit, the total energy rules, whereas short time dynamics requires the correct **q** and **p** distributions.

We showed how to obtain classical energies more in agreement with the QM ones, by applying one of three approaches: (a)

strictly fixing the total energy or (b) introducing a bias toward the wanted mode energies or (c) a combination of (a) and (b). We outlined the underlying algorithms, and we detailed, with tests on realistic cases, how the $\mathbf{q}$, $\mathbf{p}$, $E_{tot}^{(cl)}$, and $E_i^{(cl)}$ distributions depend on the sampling method. We feel that offering some new tools for the sampling of initial conditions, with well defined working and scope, can significantly improve the practice of trajectory simulations.

SUPPLEMENTARY MATERIAL

The supplementary material contains Fig. S1 about Wigner's sampling, Fig. S2 and Table S1 about one-mode sampling, and Fig. S3 about the MMS sampling.

ACKNOWLEDGMENTS

William Louis Hase passed away when this work was almost completed. We consider a privilege to have been Bill's collaborators and friends.

This work was supported by Grant No. PRA_2018_36 of the University of Pisa.

DATA AVAILABILITY

The data that support the findings of this study are available within the article and its supplementary material.

REFERENCES

[1] A. García-Vela, J. Chem. Phys. **112**, 8302 (2000).
[2] J. G. López and A. B. McCoy, Chem. Phys. **308**, 267 (2005).
[3] S. Kube, C. Lasser, and M. Weber, J. Comput. Phys. **228**, 1947 (2009).
[4] M. Paranjothy, R. Sun, Y. Zhuang, and W. L. Hase, Wiley Interdiscip. Rev.: Comput. Mol. Sci. **3**, 296 (2013).
[5] A. K. Paul, S. Kolakkandy, S. Pratihar, and W. L. Hase, in *Reaction Rate Constant Computations: Theories and Applications*, edited by K. Han and T. Chu, Computational Chemistry Series (RSC, 2013), p. 494
[6] S. Pratihar, G. L. Barnes, and W. L. Hase, Chem. Soc. Rev. **45**, 3595 (2016).
[7] M. Barbatti and K. Sen, Int. J. Quantum Chem. **116**, 762 (2016).
[8] J. Suchan, D. Hollas, B. F. E. Curchod, and P. Slavíček, Faraday Discuss. **212**, 307 (2018).
[9] G. Granucci and M. Persico, Theor. Chem. Acc. **133**, 1526 (2014).
[10] R. Crespo-Otero and M. Barbatti, Chem. Rev. **118**, 7026–7068 (2018).
[11] S. K. Min, F. Agostini, I. Tavernelli, and E. K. U. Gross, J. Phys. Chem. Lett. **8**, 3048 (2017).
[12] K. Park, J. Engelkemier, M. Persico, P. Manikandan, and W. L. Hase, J. Phys. Chem. A **115**, 6603 (2011).
[13] D. J. Tannor, *Introduction to Quantum Mechanics: A Time-Dependent Perspective* (University Science Books, Sausalito, 2007).
[14] M. Persico and G. Granucci, *Photochemistry: A Modern Theoretical Perspective* (Springer, Cham, 2018).
[15] T. Cusati, G. Granucci, M. Persico, and G. Spighi, J. Chem. Phys. **128**, 194312 (2008).
[16] E. Wigner, Phys. Rev. **40**, 749 (1932).
[17] M. Hillery, R. F. O'Connell, M. O. Scully, and E. P. Wigner, Phys. Rep. **106**, 121 (1984).
[18] S. J. Cotton and W. H. Miller, J. Phys. Chem. A **117**, 7190 (2013).
[19] L. Sun and W. L. Hase, J. Chem. Phys. **133**, 044313 (2010).
[20] K. Husimi, Proc. Phys. Math. Soc. Jpn. **22**, 264 (1940).
[21] M. Ceriotti, G. Bussi, and M. Parrinello, J. Chem. Theory Comput. **6**, 1170 (2010).
[22] M. Ruckenbauer, M. Barbatti, T. Müller, and H. Lischka, J. Phys. Chem. A **117**, 2790 (2013).
[23] D. L. Bunker and W. L. Hase, J. Chem. Phys. **59**, 4621 (1973).
[24] M. E. Muller, Commun. ACM **2**, 19 (1959).
[25] G. E. P. Box and M. E. Muller, Ann. Math. Stat. **29**, 610 (1958).
[26] G. H. Peslherbe, H. Wang, and W. L. Hase, Adv. Chem. Phys. **105**, 171 (1999).
[27] L. Sun and W. L. Hase, J. Chem. Phys. **121**, 8831 (2004).
[28] T. Shimanouchi, *Tables of Molecular Vibrational Frequencies Consolidated Volume I* (National Bureau of Standards, 1972).
[29] N. C. Craig, M. N. Ackermann, and R. A. MacPhail, J. Chem. Phys. **68**, 236 (1978).